C. R. Chimie 13 (2010) 1384–1390

Contents lists available at ScienceDirect

Comptes Rendus Chimie

www.sciencedirect.com

Full paper/Mémoire

Manganese-promoted Rh supported on a modified SBA-15 molecular sieve for ethanol synthesis from syngas. Effect of manganese loading

Guochang Chen, Xiaohui Zhang, Cun-Yue Guo, Guoqing Yuan *

Beijing National Laboratory for Molecular Sciences, Laboratory of New Materials, Institute of Chemistry, Chinese Academy of Sciences, Beijing 100190, China

ARTICLE INFO

Article history:
Received 5 November 2009
Accepted after revision 25 March 2010
Available online 15 May 2010

Keywords:
Rhodium
Manganese
CO hydrogenation
C_2 oxygenates
Ethanol
SBA-15
Syngas

ABSTRACT

A modified mesoporous molecular sieve SBA-15 possessing larger pore diameter, pore volume, and high hydrothermal stability was developed. Loaded with $RhCl_3$ and $Mn(NO_3)_2$, the as-prepared SBA-15 performed excellently in catalyzing direct conversion of syngas to ethanol. The highest perimeter of Rh-MnO interface and ethanol yield were reached at the Mn/Rh weight ratio of about 1. High CO conversion, more than 90% in the first three hours, was obtained over the catalyst 7 wt% Rh-7 wt% Mn/SBA-15. Improved catalytic performance is attributed to the increase in the amount of reducible oxide, which resulted in an enhancement of the perimeter of the Rh-MnO interface when the Mn/Rh weight ratio is about 1, and the enhanced ability of rhodium to dissociate and to hydrogenate the carbon monoxide molecule by the addition of manganese.

1. Introduction

Ethanol has found widespread use as both an energy carrier and a fuel additive. A viable route for the manufacture of ethanol is the direct conversion of syngas (Eq. (1)), which can be obtained by the gasification of coal or a renewable resource like biomass.

$$2CO(g) + 4H_2(g) \rightarrow C_2H_5OH(g) + H_2O(g) \quad (1)$$

$\Delta H^\circ_{298} = -253.6\,kJ/mol$ of ethanol
$\Delta G^\circ_{298} = -221.1\,kJ/mol$ of ethanol

However, methane is the most thermodynamically favored product (Eq. (2)), and is generally undesirable economically.

$$CO(g) + 3H_2(g) \rightarrow CH_4(g) + H_2O(g) \quad (2)$$

$\Delta H^\circ_{298} = -205.9\,kJ/mol$ of ethanol
$\Delta G^\circ_{298} = -141.9\,kJ/mol$ of ethanol

Developing new types of catalyst to synthesize ethanol from synthesis gas is very meaningful from both practical and theoretical points of view. A growing consensus regarding ethanol synthesis from syngas is that supported Rh has a great potential for the reaction, but suitable supports and promoters are needed to enhance the reactivity of Rh [1].

Most previous works have been performed over SiO_2-supported systems [2] and examples of other supports studied include Al_2O_3 [3], TiO_2 [4], NaY [5], ZrO_2 [6] and CeO_2 [7]. The mesoporous molecular sieve SBA-15 with two-dimensional hexagonally ordered arrays of channels, discovered by Zhao et al. [8], has attracted much attention for potential applications as versatile catalysts and catalyst supports [9], template [10] and separation materials [11] because of its appealing textural properties and high surface area, and appreciable thermal and hydrothermal stability. However, to our knowledge, no detailed study of the effect of Mn loading on Rh/SBA-15 catalysts on the activity of ethanol synthesis from syngas has been reported.

Here, a modified procedure for SBA-15 preparation [12] giving better reproducibility of the hexagonal porous array was adopted. The mesoporous SBA-15 was obtained

* Corresponding author.
E-mail address: yuangq@iccas.ac.cn (G. Yuan).

1631-0748/$ – see front matter
doi:10.1016/j.crci.2010.03.025

through adding promoter heteropoly acids to the template and extending crystallization time. Small amounts of phosphomolybdic acid (HPMo) can significantly enhance the crystallization process for SBA-15 formation. The reason for this is that, on the one hand, the interaction between the octahedral molybdic species and the EO moieties of the template P123 would be in favor of hydronium ions associating with them in the low concentration HCl media, which adds long-range Coulombic interactions to the coassembly process, thus enhancing the tendency for mesoscopic ordering to occur. On the other hand, the assembly of mesoporous SBA-15 may be expected to proceed through a $(S^0Mo^-)I^+$ synthesis route (where S^0 is the template P123, Mo^- is the octahedral molybdic species, and I^+ is silicate cation). Consequently, the synthesis time for the mesoporous SBA-15 formation is shortened and the corresponding degree of silicate polymerization (i.e., silanol group condensation) is expected to increase with the same crystallization time, which would result in the improvement of hydrothermal stability [12]. In comparison to the conventional synthesis method [8], the toxic liquid acids HCl concentration of reaction mixture solution is only 3.6% and the total H^+ originated from both HCl and heteropoly acids dissociation is about 4%. The SBA-15 samples prepared in the modified procedure had a BET surface area of 450–600 m^2/g. In the present research, the effect of manganese oxide loading on Rh/SBA-15 catalysts for ethanol formation from syngas is investigated in order to significantly improve the performance of catalysts for the synthesis of oxygenates from syngas, and as-prepared catalysts exhibit excellent activity and selectivity.

2. Experimental

2.1. Materials and catalyst synthesis

2.1.1. Materials

Nonionic triblock copolymer $EO_{20}PO_{70}EO_{20}$ (Pluronic P123) was purchased from Aldrich. Phosphomolybdic acid with principal composition of $H_3PO_4{\cdot}12MoO_3{\cdot}24H_2O$, was obtained from J & K Chemical. Tetraethoxysilane (TEOS) and concentrated hydrochloric acid (c-HCl, 36 wt%) were provided by Shanghai Chemical Regent Company of China. Rhodium chloride ($RhCl_3{\cdot}3H_2O$) was purchased from Beijing Chemical Agents Plant. $Mn(NO_3)_2$ was obtained from Tianjin Tianhe Chemical Agents Plant.

2.1.2. Synthesis of SBA-15

A modified procedure for SBA-15 preparation [12] affording larger pore diameter, pore volume, and higher hydrothermal stability was adopted. In a typical synthesis batch, 3.0 g of P123 was dissolved in 78.75 mL of distilled water with vigorously stirring at room temperature for 3 h, then 0.48 g of HPMo (the molar ratio of Si/Mo was 12.4) was added into the solution. After the P123 and HPMo were dissolved completely, 6.9 mL of TEOS and 0.56 mL of c-HCl were added dropwise to the above mixture solution. The chemical composition of the reaction mixture was: 3 g P123; 0.031 mol TEOS; 0.00021 mol heteropoly acids; 0.0065 mol HCl; 4.37 mol H_2O. Subsequently, the mixture was stirred at 313 K for 24 h and thermally treated at 373 K for 48 h. The reaction products were filtered, washed, and dried at 318 K for 48 h. Finally, the samples were calcined at 823 K in air for 8 h with a slow temperature increase of 1 $Kmin^{-1}$.

2.1.3. Catalyst synthesis

Catalysts were prepared by impregnating SBA-15 with an aqueous solution of $RhCl_3{\cdot}3H_2O$ and/or $Mn(NO_3)_2$ via the incipient wetness technique. The impregnates were subsequently dried in air at 383 K for 2 h. Calcination was carried out at 773 K for 12 h (heating rate of 10 K min^{-1}). The rhodium content and the weight percent of manganese is listed in related tables and figures.

2.2. Catalyst characterization

2.2.1. N_2 adsorption-desorption

N_2 adsorption-desorption isotherms were obtained at 77 K on an Omnisorp-100CX apparatus (USA). Prior to analysis, all samples were degassed in high vacuum for 2 h at 523 K. BET surface areas were calculated from the linear part of the BET plot. The pore size distribution (PSD) was calculated by the Barret-Joyner-Halenda model, and the total pore volumes were estimated from the N_2 uptake at $P/P_0 = 0.994$.

2.2.2. X-ray powder diffraction (XRD)

XRD patterns were recorded on a Rigaku D/max 2550PC diffractometer (Rigaku, Japan) using Cu Ka radiation, operating at 40 kV and 300 mA.

2.2.3. Transmission electron microscopy (TEM)

TEM images were obtained on a JEM-2010HR microscope (JEOL, Japan). Samples for TEM studies were prepared by dipping a carbon-coated copper grid into a suspension of mesoporous material in ethanol that was pre-sonicated for 10 min.

2.2.4. Temperature programmed reduction (TPR)

TPR experiments were carried out on a Micromeritics TPD/TPR 2900 apparatus. The catalyst (about 40 mg) was pretreated under dry air at 383 K for 1 h. The TPR profile was recorded by heating the sample from room temperature to 973 K at a rate of 10 K min^{-1} under a H_2/Ar (10% v/v) flow.

2.2.5. Temperature programmed surface reaction (TPSR) of adsorbed CO

TPSR experiments of CO adsorbed were performed using a U-shaped quartz reactor connected to a Baltzer Prisma QMS200TM mass spectrometer. The experimental procedure was as follows: The reactor was loaded with about 50 mg of sample (0.25–0.30 mm particle size). After the sample was reduced according to the process described above, the microreactor was swept with He for 0.5 h and then cooled down to 323 K. CO was adsorbed by flowing a CO/He (5% v/v) mixture at 298 K for 30 min. Physisorbed CO was purged with Ar for 30 min. Finally, the temperature was linearly increased from 298 to 923 K at a heating rate of 10 K min^{-1} under a H_2/Ar (10% v/v) flow. The signals of H_2 (m/z = 2), CO (m/z = 28), CH_4 (m/z = 16), H_2O (m/z = 18),

and Ar(m/z = 40) were simultaneously recorded with the mass spectrometer.

2.3. Catalytic measurements

CO hydrogenation reactions were performed using a high-pressure fixed-bed microreactor (stainless steel 316#, 200 mm length and 4 mm internal diameter). First, 0.5 g catalyst was reduced in situ at 673 K (heating rate of 1 K min^{-1}) for 16 h in a flow of H_2/N_2 (1:9) at a rate of 100 cm^3 min^{-1}. The reactor was then cooled down and the gas flow was switched to 75 cm^3 min^{-1} (or 60 cm^3 min^{-1} or 45 cm^3 min^{-1}) of syngas (molar ratio $H_2/CO = 2$). The system was pressurized at 1.0 MPa and heated to the desired temperatures at a heating ramp of 10 K min^{-1}. Temperature was measured with a type-K thermocouple buried in the catalytic bed. Flow rates were controlled using a Brooks 5850 TR Series mass flow controllers. All experimental variables were carefully controlled to ensure identical reaction conditions when testing catalysts. Some recommendations and criteria proposed by Pérez-Ramírez et al. [13] were followed to ensure accurate measurements.

Product analysis was performed online with a gas chromatograph (GC2014) equipped with TCD and FID detectors and two in-series fused silica capillary columns: SPB-5 (60 m × 0.53 mm) and Supel-Q Plot (30 m × 0.53 mm). It was possible to analyze inorganic gases such as H_2, CO and CO_2 etc., C_1–C_{20} hydrocarbons, C_1–C_{10} alcohols, and other oxygenated compounds. The identification of reaction products and gas chromatograph calibration were accomplished using gas chromatography-mass spectrometry (GC-MS) and quantitative standard solutions from AccuStandard.

3. Results and discussion

3.1. CO hydrogenation results

Manganese loading plays a crucial role in promoting the yield of oxygenated compounds, as shown in Table 1. Only a trace of ethanol was produced on the unpromoted Rh/SBA-15 catalyst, although high CO conversion was observed. It indicated that a completely promoter-free rhodium catalyst could not produce ethanol. When the Mn/Rh ratio increased from 0.5 to 2, the average CO conversion increased from 8.2 to a maximum 21.9% at Mn/Rh = 1, then decreasing to 9.3%. The yield of liquid products also presented the same trend, increasing from 120.6 to a maximum 508.4 g (kg-cat h)$^{-1}$ at Mn/Rh = 1, then decreasing to 182.4 g (kg-cat h)$^{-1}$.

The effects of flow rate of syngas on the conversion and selectivity with the 5 wt% Rh-5 wt% Mn/SBA-15 catalyst are summarized in Table 2. As expected, CO conversion decreased with increasing flow rate. Obviously, the product selectivities are also affected. Table 2 illustrates that increasing syngas flow rate from 60 to 90 cm^3 min^{-1} decreased the average CO conversion from 25.0 to 17.6% while simultaneously increasing the ethanol selectivity from 8.7% at a flow rate of 60 cm^3 min^{-1} to a maximum 12.9% at 75 cm^3 min^{-1} and then decreasing to 11.6% at 90 cm^3 min^{-1}.

The effect of Rh loading on the activity and selectivity of Mn promoted Rh/SBA-15 catalysts (Mn/Rh weight ratio = 1) is shown in Table 3. As expected, CO conversion over the catalysts increased with increasing Rh loading. However, ethanol selectivity reached a maximum for 5 wt%Rh-5 wt%Mn/SBA-15, the formation of ethanol being suppressed at higher Rh loading. Fig. 1 illustrates how the CO conversion changed with time over a 13-h time interval. It should be noted that the catalyst 7 wt% Rh-7 wt% Mn/SBA-15 exhibits excellent activity. CO conversion is more than 90% in the first 3 h, and average CO conversion is 64.3%, as shown in Table 3. The increased catalytic performance is attributed to the increase in the amount of reducible oxide which resulted in an enhancement of the perimeter of the Rh-MnO interface when the Mn/Rh weight ratio is about 1, and the enhanced ability of rhodium to dissociate and to hydrogenate the carbon monoxide molecule by the addition of manganese. This point will be discussed in following sections.

3.2. Characterization of the catalysts by XRD

Fig. 2 presents the XRD patterns for the SBA-15-supported Rh samples with different loading amounts of manganese. In the case of parent SBA-15, three well resolved diffraction peaks, which are indexed as the (1 0 0), (1 1 0) and (2 0 0) reflections, associated with p6 mm hexagonal symmetry [8], are observed. With increasing loading of manganese, although peaks (1 1 0) and (2 0 0) became unobservable, indicating the de-organization at long range of the mesoporous structure, the peak (1 0 0) was clearly observed, which indicated that the hexagonal patterns were still retained on the impregnated catalysts.

Table 1
Effect of Mn loading on Rh-Mn/SBA-15 catalysts for syngas conversion.

Catalyst	Conversion (%)	%Selectivity							Y g/(kg-cat h)
		CH_4	CO_2	CH_3OH	C_2H_5OH	C_3H_7OH	CH_3CHO	C_4H_9OH	
5%Rh/SBA-15	68.9	36.6	62.8	0.4	0.2	0.01	0	0	–
5%Rh-2.5%Mn/SBA-15	8.2	47.2	26.7	0.3	21.5	4.0	0.1	0.2	120.6
5%Rh-5%Mn/SBA-15	21.9	61.6	23.8	1.2	12.9	0.4	0.1	0.1	508.4
5%Rh-7.5%Mn/SBA-15	19.8	53.4	25.8	0.8	19.0	0.7	0.2	0.1	368.4
5%Rh-10%Mn/SBA-15	9.3	53.3	20.4	0.3	22.2	3.3	0.2	0.4	182.4

Nominal conditions are $T = 573$ K, $P = 1$ MPa, 0.50 g catalyst, H_2:CO = 2:1, syngas flow = 75 cm^3(STP)min^{-1}. Conversion (%) = $\Sigma n_i M_i \times 100/M_{CO}$ and selectivity = $n_i M_i / \Sigma n_i M_i$ where n_i is the number of carbon atoms in product i, M_i is the mole percent of product i measured, and M_{CO} is the mole percent of carbon monoxide in the feed. Y implies all the liquid products such as methanol, ethanol, propanol, acetaldehyde, etc. Reaction time: 13 h.

Table 2
Effects of flow rate on the reactions of syngas over a 5wt% Rh-5 wt% Mn/SBA-15-HPMo catalyst (reaction time: 13 h).

Condition	1	2	3
T (K)	573	573	573
P (MPa)	1	1	1
$H_2 + CO$ ($cm^3\ min^{-1}$)	60	75	90
H_2/CO	2:1	2:1	2:1
Conversion (%)	25.0	21.9	17.6
Selectivities (%)			
CH_4	58.2	61.6	63.2
CO_2	31.5	23.8	22.6
CH_3OH	1	1.2	1.5
C_2H_5OH	8.7	12.9	11.6
C_3H_7OH	0.42	0.5	1.0
C_4H_9OH	0.03	0.1	0.02
CH_3CHO	0.1	0.1	0.1

3.3. Characterization of the catalysts by N_2 adsorption-desorption isotherms

Table 4 gives the textural properties of parent SBA-15 and 5 wt%Rh-5 wt%Mn/SBA-15 by the N_2 adsorption-desorption isotherms. Impregnation of SBA-15 with $RhCl_3$ and $Mn(NO_3)_2$ produces a decrease in specific surface area which is attributed to clogging support pores by $RhCl_3$ and $Mn(NO_3)_2$ species that makes them inaccessible for nitrogen adsorption. This phenomenon was already observed by Laugel et al. [14]. After $RhCl_3$ and $Mn(NO_3)_2$ introduction, the average volume of the catalysts becomes smaller but the average pore diameter does not change. These results suggest that the $RhCl_3$ and $Mn(NO_3)_2$ species are probably located inside the mesoporous channels of SBA-15 rather than dispersing on the wall surface. This is consistent with the results of Wang et al. [15], who examined the SBA-15-supported iron phosphate catalyst for partial oxidation of methane to formaldehyde, and believed that iron phosphate ($FePO_4$) species with loading amount lower than 40 wt% were located inside the mesoporous channels of SBA-15.

3.4. Characterization of the catalysts by TEM

TEM observations further support the encapsulation of $RhCl_3$ and $Mn(NO_3)_2$ species within the mesopores. As typical example, TEM images of the 5 wt%Rh-5 wt%Mn/SBA-15 are shown in Fig. 3. The hexagonal array of mesoporous channels is clearly observed. Moreover, small clusters encapsulated inside the mesoporous channels can also be discerned when Figs. 3B and C are compared. No large particles locating outside the mesopores are observed in the case of 5 wt% Rh-5 wt% Mn/SBA –15 (Figs. 3A and B).

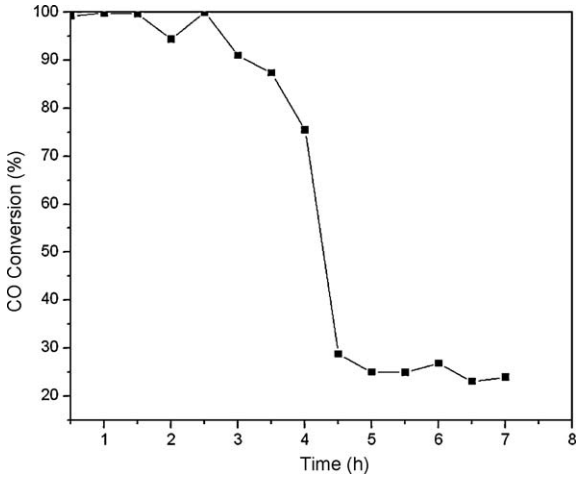

Fig. 1. CO Conversion over 7 wt% Rh-7 wt% Mn/SBA-15.

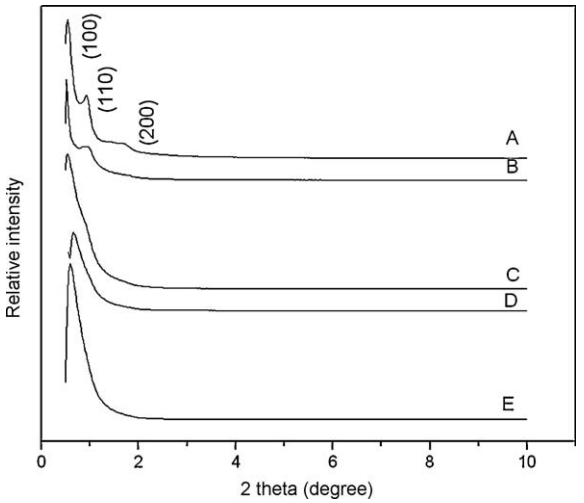

Fig. 2. XRD patterns at low diffraction angles: (A) SBA-15, (B) 5 wt%Rh-0.5 wt%Mn/SBA-15, (C) 5 wt%Rh-2.5 wt%Mn/SBA-15, (D) 5 wt%Rh-5 wt%Mn/SBA-15 and (E) 5 wt%Rh-7.5 wt%Mn/SBA-15.

Table 3
Effect of Rh loading on syngas conversion over Rh-Mn/SBA-15 catalysts (Rh/Mn = 1:1). Reaction time: 13 h.

Catalyst	Conversion (%)	%Selectivity				
		CH_4	CO_2	CH_3OH	C_2H_5OH	C_3H_7OH
1%Rh-1%Mn/SBA-15	3.4	53.6	43.1	2.0	1.3	0.2
3%Rh-3%Mn/SBA-15	10.9	74.6	21.8	1.4	2.1	0.07
5%Rh-5%Mn-/SBA-15	21.9	61.6	23.8	1.2	12.9	0.5
7%Rh-7%Mn/SBA-15	64.2	91.8	3.9	0.2	4.0	0.1

Nominal conditions are $T = 573$ K, $P = 1$ MPa, 0.50 g catalyst, H_2:CO 2:1, syngas flow = 75 cm^3(STP)min^{-1}. Conversion (%) = $\Sigma n_i M_i \times 100/M_{CO}$ and selectivity = $n_i M_i/\Sigma n_i M_i$ where n_i is the number of carbon atoms in product i, M_i is the mole percent of product i measured, and M_{CO} is the mole percent of carbon monoxide in the feed.

Table 4
Porous properties of parent SBA-15 and 5 wt%Rh-5 wt%Mn/SBA-15.

Sample	Surface area ($m^2 g^{-1}$)	Pore volume ($cm^3 g^{-1}$)	Pore diameter (nm)	Crystal Structure[a]
SBA-15	495.2	1.2	8.6	Hexagonal
5 wt%Rh-5 wt%Mn/SBA-15	363.6	0.9	8.7	Hexagonal

[a] Crystal structure was confirmed by XRD.

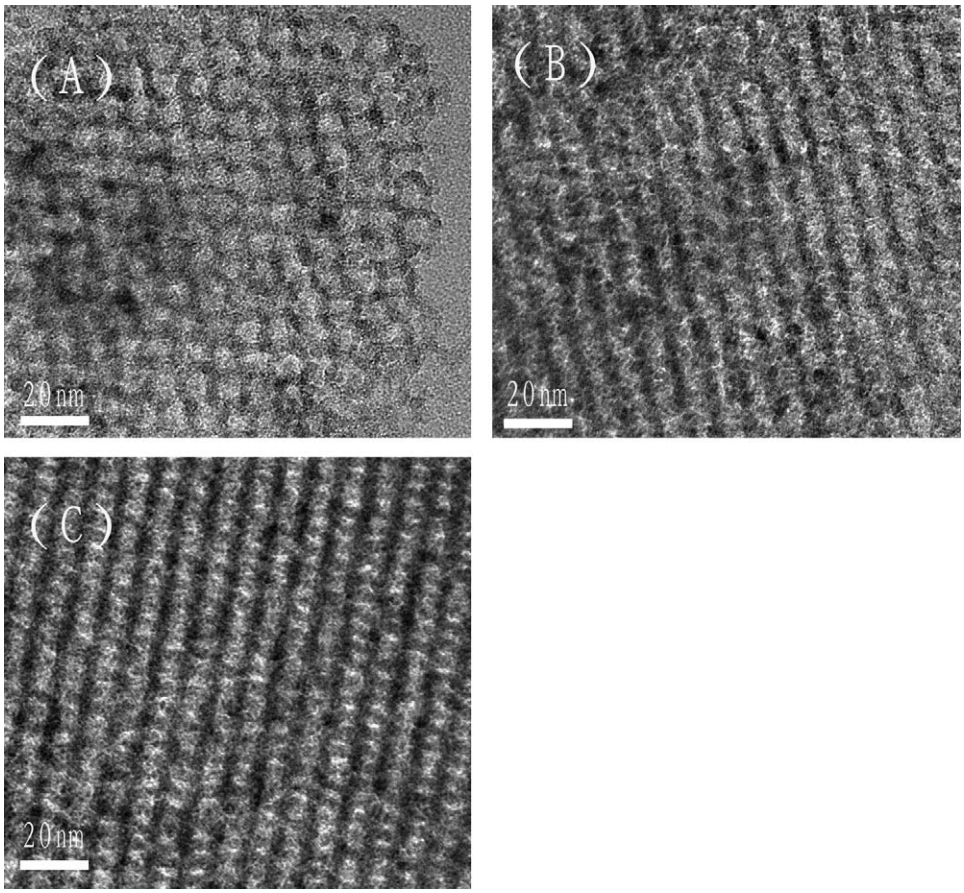

Fig. 3. TEM images of the 5 wt%Rh-5 wt%Mn/SBA-15 (A) and (B), and SBA-15 (C). (A) Taken with the beam parallel to the pore direction and (B) and (C) taken with the beam perpendicular to the pore direction.

3.5. Characterization of the catalysts by TPR

Fig. 4 shows TPR profiles for the catalysts investigated. The Rh-free Mn-supported SBA-15 sample exhibits two small reduction peaks at about 456 and 783 K, which can be ascribed to the reduction sequence $MnO_2 \rightarrow Mn_3O_4 \rightarrow MnO$ [16]. This is based on thermodynamic arguments and experimental evidence from the literature [17]. The Rh/SBA-15 catalyst without promoter gives a reduction peak centered at 370 K, which corresponds to the reduction of Rh^{3+} to give metallic rhodium. The addition of the Mn promoter changed the reducibility of Rh and Mn oxides. Upon increasing the manganese loading, the reducibility of the rhodium was decreased, shifting the maximum of reduction peak from 370 K for the unpromoted catalyst to 400, 410 and 410 K for the samples with Mn/Rh = 0.5, 1 and 2 (Fig. 4C, D, E), respectively. At the same time, a remarkable shift to a lower reduction temperature of the manganese oxide is observed. The manganese oxide reduction peaks seem to overlap with that of the rhodium oxide in the case of 5 wt%Rh-5 wt%Mn/SBA-15 (Fig. 4C). The ability of a noble metal oxide to accelerate the reduction of a second surface metal oxide species with which it is in intimate contact has been reported previously [18]. Metallic rhodium provides sites for hydrogen adsorption and dissociation with extremely low activation energy. If MnO_x particles are close enough to the metal sites, their reduction by atomic hydrogen takes place at a lower temperature than if molecular hydrogen has to interact with MnO_2, and hence the reducibility of Mn

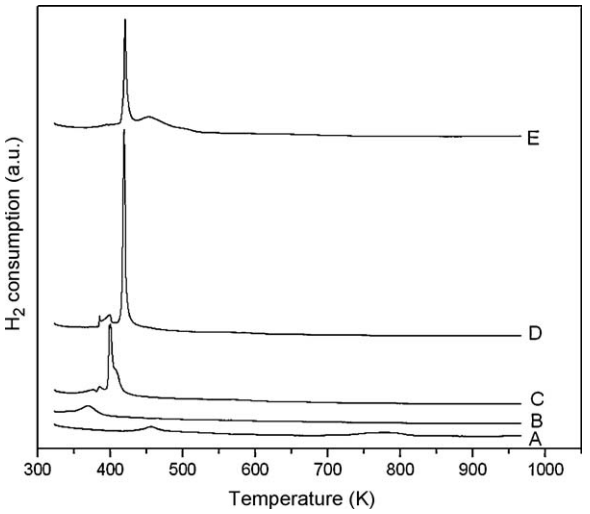

Fig. 4. TPR profiles: (A) 5 wt%Mn/SBA-15, (B) 5 wt%Rh/SBA-15, (C) 5 wt %Rh-2.5 wt%Mn/SBA-15, (D) 5 wt%Rh-5 wt%Mn/SBA-15 and (D) 5 wt%Rh-10 wt%Mn/SBA-15.

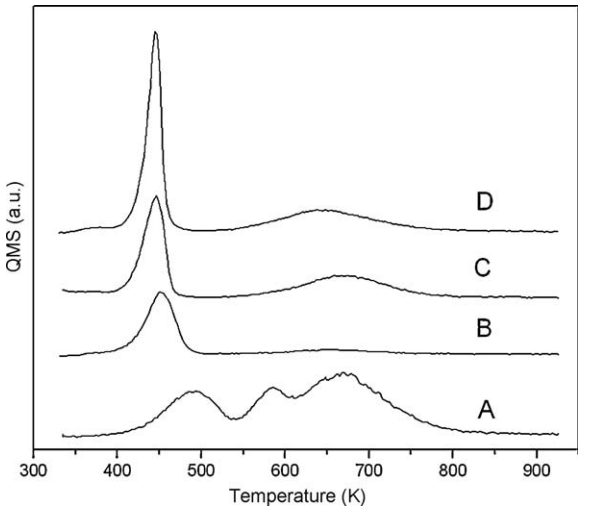

Fig. 5. Methane formation spectra during TPSR of adsorbed CO under H_2 flow over catalysts: (A) 5 wt%Rh/SBA-15, (B) 5 wt%Rh-2.5 wt.%Mn/SBA-15, (C) 5 wt% Rh -5wt%Mn/SBA-15, (D) 5 wt%Rh-10 wt%Mn/SBA-15.

oxides is enhanced by the close proximity of Rh [16]. These findings clearly support that a close interaction between Rh and Mn oxides existed in our catalysts.

With increasing manganese loading, the H_2 consumption increased to maximum at Mn/Rh = 1, and then decreased. The enhancement of H_2 consumption (Fig. 4D) was related to the increase in the amount of reducible oxide [19], which resulted in an enhancement of the perimeter of the Rh-MnO interface responsible for CO insertion [1]. It was one of reasons for the increased catalytic performances when the Mn/Rh weight ratio is about 1. This can be explained by taking into account two aspects: the amount of promoter added and the size of the MnO particles deposited. When the Mn content is low, the MnO particles deposited over the rhodium surface are rather small, and any increase in promoter loading would be reflected as an enhancement of the perimeter of the Rh-MnO interface, thus increasing the number of active CO insertion sites. However, when the Mn/Rh ratio is higher than 1, large MnO patches are deposited over the rhodium surface, and the Rh-MnO interface perimeter is diminished. So there exists an optimum promoter loading, that is Mn/Rh (weight ratio) = 1, at which the Rh-MnO interface has the highest perimeter.

3.6. Characterization of the catalysts by TPSR

The reactivity of chemisorbed CO under H_2 flow provides useful information about the ability of rhodium to dissociate and to hydrogenate the carbon monoxide molecule. Since the hydrogenation of carbon into methane is very fast on Rh-Mn based catalysts, methane production can be used as a tool for measuring the CO dissociation over such catalysts. Fig. 5 shows the production of CH_4 when the hydrogenation of chemisorbed CO is carried out from room temperature to 900 K.

Two effects were observed when manganese was added to the unpromoted Rh/SBA-15 catalyst. The first observation was that the temperature at which methane started to be formed and the corresponding maximum were shifted toward lower temperatures with increasing promoter loading. The methane formation peak shifted from 490 to 450, 440 and 430 K for Mn/Rh = 0.5, 1 and 2. This indicates that the addition of manganese increased the ability of rhodium to dissociate the CO molecules, which can strongly affect catalytic performance. This is consistent with the literature [20]. It can be explained by taking into account electronic effects. According to the well known model of CO adsorption over metal surfaces first postulated by Blyholder [21], the carbon monoxide-to-metal bond is considered to result from a charge transfer from the HOMO of CO (5σ) into a free σ symmetry d orbital of the metal and an electron back-donation from an occupied π symmetry d orbital of the metal into the unoccupied $2\pi^*$ antibonding orbital of CO. This back-donation to the CO antibonding orbital weakens the CO bond. As an electron acceptor, the oxophilic promoter Mn ions coadsorbed CO with Rh on the same surface [20], therefore the back-donation to the antibonding molecular orbital is enhanced and, in turn, the ability of rhodium to dissociate the CO molecule is increased. The second observation was the increase in the methane peak area from B to D. In principle, it would be expected that increasing the amount of promoter could partially block the rhodium surface, thereby diminishing the number of active sites. Accordingly, the increment in the CO dissociate would be due to a higher catalytic activity per rhodium site, i.e., a higher turn over frequency. Sachtler and Ichikawa [20] believed that on the Rh-promoter interface the adsorbed CO could be readily dissociated. This effect became stronger as the Mn/Rh weight ratio increases.

So the increased ability of rhodium to dissociate the CO molecules by the addition of manganese was another reason for the improved catalytic performances of Rh-Mn/SBA-15.

4. Conclusions

The modified SBA-15 molecular sieves, support for manganese-promoted Rh catalysts (Mn/Rh = 0, 0.5, 1 and 2, weight ratio), were used in the synthesis of ethanol from syngas. The optimum Mn/Rh ratio was found to be around 1 for ethanol formation. The CO conversion is more than 90% in the first three hours over the catalyst 7 wt% Rh-7 wt% Mn/SBA-15. The improved catalytic performance is attributed to the increase in the amount of reducible oxide, which resulted in an enhancement of the perimeter of the Rh-MnO interface when the Mn/Rh weight ratio is about 1, and the enhanced ability of rhodium to dissociate and to hydrogenate the carbon monoxide molecule by the addition of manganese.

References

[1] (a) R. Burch, M.I. Petch, Appl. Catal. A 88 (1992) 39;
(b) R. Burch, M.I. Petch, Appl. Catal. A 88 (1992) 77;
(c) P. Gronchi, E. Tempesti, C. Mazzocchia, Appl. Catal. A 120 (1994) 115;
(d) R. Burch, M.J. Hayes, J. Catal 165 (1997) 249;
(e) C. Mazzocchia, P. Gronchi, A. Kaddouri, E. Tempesti, L. Zanderighi, A. Kiennemann, J. Mol. Catal. A Chem 165 (2001) 219;
(f) H. Ma, Z. Yuan, Y. Wang, X. Bao, Surf. Interface Anal 32 (2001) 224;
(g) M. Ojeda, M.L. Granados, S. Rojas, P. Terreros, F.J. Garcia-Garcia, J.L.G. Fierro, Appl. Catal. A 261 (2004) 47;
(h) M.A. Haider, M.R. Gogate, R.J. Davis, J. Catal 261 (2009) 9.
[2] (a) M. Bowker, Catal. Today 15 (1992) 77;
(b) D. Jiang, Y. Ding, Z. Pan, X. Li, G. Jiao, J. Li, W. Chen, H. Luo, Appl. Catal. A 331 (2007) 70.
[3] P. Basu, D. Panayotov, J.T. Yates, J. Am. Chem. Soc 110 (1988) 2074.
[4] Z.L. Zhang, A. Kladi, X.E. Verykios, J. Catal 156 (1995) 37.
[5] T.T.T. Wong, A.Y. Stakheev, W.M.H. Sachtler, J. Phys. Chem 96 (1992) 7733.
[6] J.A. Anderson, M.M. Khader, J. Mol. Catal. A Chem 105 (1996) 175.
[7] J.C. Lavalley, J. Saussey, J. Lamotte, R. Breault, J.P. Hindermann, A. Kiennemann, J. Phys. Chem 94 (1990) 5941.
[8] D. Zhao, J. Feng, Q. Huo, N. Melosh, G. Fredrickson, B.F. Chmelka, G.D. Stucky, Science 279 (1998) 548.
[9] A. Taguchi, F. Schüth, Micropor. Mesopor. Mater 77 (2005) 1.
[10] K.K. Zhu, B. Yue, W.Z. Zhou, H.Y. He, Chem. Commun (2003) 98.
[11] Y. Ueno, A. Tate, O. Niwa, H.S. Zhou, T. Yamada, I. Honma, Chem. Commun (2004) 746.
[12] (a) D. Zhao, J. Sun, Q. Li, G.D. Stucky, Chem. Mater 12 (2000) 275;
(b) Y. Luo, Z. Hou, R. Li, X. Zheng, Micropor. Mesopor. Mater 109 (2008) 585.
[13] J. Pérez-Ramírez, R.J. Berger, G. Mul, F. Kapteijn, J.A. Moulijn, Catal. Today 60 (2000) 93.
[14] G. Laugel, J. Arichi, P. Bernhardt, M. Molière, A. Kiennemann, F. Garin, B. Louis, C. R. Chimie 12 (2009) 731.
[15] Y. Wang, X. Wang, Z. Su, Q. Guo, Q. Tang, Q. Zhang, H. Wan, Catal. Today 93–95 (2004) 155.
[16] H. Treviño, G.D. Lei, W.M.H. Sachtler, J. Catal 154 (1995) 245.
[17] K.P. de Jong, J.H.E. Glezer, H.P.C.E. Kuipers, A. Knoester, C.A. Emeis, J. Catal 124 (1990) 520.
[18] (a) V. Schünemann, H. Treviño, G.D. Lei, D.C. Tomczak, W.M.H. Sachtler, K. Fogash, J.A. Dumesic, J. Catal 153 (1995) 144;
(b) B.J. Kip, E.G.F. Hermans, J.H.M.C. van Wolput, N.M.A. Hermans, J. van Grondelle, R. Prins, Appl. Catal 35 (1987) 109.
[19] H.Y. Luo, P.Z. Lin, S.B. Xie, H.W. Zhou, C.H. Xu, S.Y. Huang, L.W. Lin, D.B. Liang, P.L. Yin, Q. Xin, J. Mol. Catal. A Chem 122 (1997) 115.
[20] W.M.H. Sachtler, M. Ichikawa, J. Phys. Chem 90 (1986) 4752.
[21] G. Blyholder, J. Phys. Chem 68 (1964) 2772.